

PAPER • OPEN ACCESS

RKDG method for 2D gas dynamics simulation on uniform rectangular meshes

To cite this article: Victoria Korchagova *et al* 2019 *J. Phys.: Conf. Ser.* **1348** 012098

View the [article online](#) for updates and enhancements.



IOP | ebooks™

Bringing you innovative digital publishing with leading voices to create your essential collection of books in STEM research.

Start exploring the collection - download the first chapter of every title for free.

RKDG method for 2D gas dynamics simulation on uniform rectangular meshes

Victoria Korchagova^{1,2,4}, Ivan Fufaev³, Vladimir Lukin^{1,2,3},
Ilya Marchevsky^{1,2} and Sofya Sautkina¹

¹ Bauman Moscow State Technical University, 2-nd Baumanskaya st. 5, Moscow, 105005 Russia

² Ivannikov Institute for System Programming of the RAS, Alexander Solzhenitsyn st. 25, Moscow, 109004 Russia

³ Keldysh Institute of Applied Mathematics RAS, Miusskaya sq. 4, Moscow, 125047 Russia

⁴ E-mail: v.korchagova@ispras.ru

Abstract. This paper is devoted to a numerical simulation of 2D gas dynamics flows on uniform rectangular meshes using the Runge - Kutta - Discontinuous - Galerkin (RKDG) method. The RKDG algorithm was implemented with in-house C++ code based on the experience in the investigation of 1D case. The advantage of the RKDG method over the most popular finite volume method (FVM) is discussed: three basis functions being applied in the framework of the RKDG approach lead to a considerable decrease of the numerical dissipation rate with respect to FVM. The results of the acoustic pulse simulation on a sufficiently coarse mesh with the piecewise-linear approximation show a good agreement with the analytical solution in contrast to the FVM numerical solution. For the Sod problem, the results of the discontinuities propagation illustrate the dependence of the scheme resolution on the numerical fluxes, troubled cell indicator and the limitation technique choice. The possibility to resolve strong shocks is demonstrated with the Sedov cylindrical explosion test.

1. Introduction

The Runge — Kutta Discontinuous Galerkin (RKDG) method is one of the most popular high order methods for handling the problems with a discontinuous solution. Its compact stencil provides operating with complex geometry, hence RKDG is widespread in aeroacoustics [1, 2] and hydrodynamics [3].

According to the Godunov theorem [4], this algorithm requires additional monotization for suppressing spurious oscillations with so-called limiters [5]. When these limiters are applied in a region with a smooth solution, some of them may lead to a decreased order of accuracy. Therefore, special indicators of troubled cells have been developed. However, an imperfection of an indicating technology resulting in mistaken limiter usage remains an important problem.

In case of multidimensional simulation on unstructured meshes, one usually uses the minmod-based limiters, *e.g.* MUSCL [6, 7]. Their widespread usage is mostly related to the ease of implementation. Nevertheless, most of them, especially general kinds, provide a rather low quality of discontinuities resolution.

Recent investigations for 1D case [8, 9] show a high efficiency of the limiters based on the Weighted Essentially Non-Oscillatory (WENO) approach. The original idea of the WENO



reconstruction is unsuitable for multidimensional modelling since it requires too wide a stencil for the high order approximation [10]. However, modifications of the concept with a compact approximation stencil containing only immediate neighbours of a cell have been developed [11, 12].

In this paper, we compare the simple WENO (WENO_S, [11]) limiter with the general MUSCL limiter in order to estimate the efficiency of the minmod and WENO approaches using the simplest implementations from each class. The goal of the current study is to develop a background for the further research with unstructured meshes [13].

2. Governing equations

Let us consider a perfect compressible gas characterized with density ρ , velocity $\mathbf{v} = [u, v, w]^T$, pressure p , specific heat capacity γ . The flow of such gas is described by the system of 2D Euler equations [14]:

$$\frac{\partial \mathbf{U}}{\partial t} + \frac{\partial \mathbf{F}(\mathbf{U})}{\partial x} + \frac{\partial \mathbf{G}(\mathbf{U})}{\partial y} = \mathbf{0}, \quad (1)$$

with

$$\begin{aligned} \mathbf{U} &= [\rho, \rho u, \rho v, \rho w, e]^T, \\ \mathbf{F} &= [\rho u, \rho u^2 + p, \rho uv, \rho uw, (e + p)u]^T, \\ \mathbf{G} &= [\rho v, \rho vu, \rho v^2 + p, \rho vw, (e + p)v]^T. \end{aligned} \quad (2)$$

where \mathbf{U} is the conservative variables vector, \mathbf{F} , \mathbf{G} are the vectors of fluxes, $e = \rho\varepsilon + \frac{1}{2}\rho(u^2 + v^2 + w^2)$ is a volumetric total energy, ε is a specific internal energy. The mathematical model should be closed with an Equation of State (EoS) for the perfect gas:

$$p = (\gamma - 1)\rho\varepsilon. \quad (3)$$

The system (1)–(2) has the following quasilinear non-conservative form:

$$\frac{\partial \mathbf{U}}{\partial t} + A \frac{\partial \mathbf{U}}{\partial x} + B \frac{\partial \mathbf{U}}{\partial y} = \mathbf{0}.$$

This system is hyperbolic, and matrices A and B can be diagonalized using the corresponding left and right eigenvectors matrices:

$$\begin{aligned} A &= \Omega_R^A \Lambda^A \Omega_L^A, & \Omega_R^A &= (\Omega_L^A)^{-1}, \\ B &= \Omega_R^B \Lambda^B \Omega_L^B, & \Omega_R^B &= (\Omega_L^B)^{-1}, \end{aligned} \quad (4)$$

where $\Lambda^j = \text{diag}[\lambda_1^j, \dots, \lambda_5^j]$, $j = A, B$, — the diagonal eigenvalue matrices for A and B ; Ω_R^j, Ω_L^j are the right and left eigenvectors matrices, respectively.

The equations (1) are considered on $[0; L_x] \times [0; L_y] \times (0; T]$ space and time domain with the initial conditions

$$\mathbf{U}(x, y, 0) = \mathbf{U}_0(x, y). \quad (5)$$

3. Overview of numerical method

3.1. Spatial discretization

Let us introduce the uniform spatial mesh with steps $h_x = L_x/N_x$ and $h_y = L_y/N_y$ which consists of $N_x \cdot N_y$ cells I_{ij} centered at $(x_i, y_j) = ((i - 1/2)h_x, (j - 1/2)h_y)$ with corners at points

$$(x_{i\pm 1/2}, y_{j\pm 1/2}) = (x_i \pm h/2, y_j \pm h/2), \quad i = \overline{1, N_x}, \quad j = \overline{1, N_y}.$$

We consider the space of piecewise-continuous functions $V_h^k = \{p: p|_{I_{ij}} \in \mathbf{P}_k(I_{ij})\}$, which are polynomials of degree at most k with respect to x and y defined on each cell I_{ij} . The system (1), (5) can be approximated as follows: each equation should be multiplied by the test function $v(x, y) \in V_h^k$ and integrated over the cell I_{ij} [5].

We define the approximate solution as

$$\mathbf{U}_h(x, y, t) = \sum_{i,j} \sum_{r=0}^2 \mathbf{U}_{ij}^{(r)}(t) \phi_{ij}^{(r)}(x, y),$$

where $\{\phi_{ij}^{(r)}(x, y)\}_{r=0}^2$ is the orthonormal basis defined for each cell I_{ij} by the following way:

$$\phi_{ij}^{(0)}(x, y) = \frac{1}{\sqrt{h_x h_y}}, \quad \phi_{ij}^{(1)}(x, y) = \sqrt{\frac{12}{h_x^3 h_y}} (x - x_i), \quad \phi_{ij}^{(2)}(x, y) = \sqrt{\frac{12}{h_x h_y^3}} (y - y_j).$$

Being interested in the numerical solution, hereinafter we omit the subscript h . After replacing $v(x, y)$ with the basis functions, the following system of ODE for solution coefficients $\mathbf{U}_{ij}^{(r)}$, $r = 0, 1, 2$, is obtained:

$$\begin{aligned} \frac{d\mathbf{U}_{ij}^{(r)}(t)}{dt} &= \int_{I_{ij}} \mathbf{F}_{ij} \frac{\partial \phi_{ij}^{(r)}}{\partial x} dx dy + \int_{I_{ij}} \mathbf{G}_{ij} \frac{\partial \phi_{ij}^{(r)}}{\partial y} dx dy - \\ &\quad - \int_{\partial I_{ij,R}} \mathbf{F}_{ij} \phi_{ij}^{(r)} dx + \int_{\partial I_{ij,L}} \mathbf{F}_{ij} \phi_{ij}^{(r)} dx - \int_{\partial I_{ij,T}} \mathbf{G}_{ij} \phi_{ij}^{(r)} dy + \int_{\partial I_{ij,B}} \mathbf{G}_{ij} \phi_{ij}^{(r)} dy, \quad (6) \\ \mathbf{U}_{ij}^{(r)}(0) &= \int_{I_{ij}} \mathbf{U}_0(x, y) \phi_{ij}^{(r)} dx dy, \quad k = 1, \dots, N_x \cdot N_y, \quad r = 0, 1, 2. \end{aligned}$$

Here $\mathbf{F}_{ij} = \mathbf{F}(\mathbf{U}_{ij}(x, y, t))$, $\mathbf{G}_{ij} = \mathbf{G}(\mathbf{U}_{ij}(x, y, t))$; $\partial I_{ij,L}$, $\partial I_{ij,R}$, $\partial I_{ij,T}$ and $\partial I_{ij,B}$ denote the left, right, top and bottom boundaries of the cell I_{ij} , respectively.

3.2. Time discretization

In case of high accuracy order space discretization, it is necessary to choose a consistent time integration method. We use the second order explicit TVD Runge — Kutta method [15]:

$$\begin{aligned} \mathbf{U}^* &= \mathbf{U}^n + \tau \mathbf{L}_h(\mathbf{U}^n), \\ \mathbf{U}^{n+1} &= \frac{1}{2} \mathbf{U}^n + \frac{1}{2} \mathbf{U}^* + \frac{1}{2} \tau \mathbf{L}_h(\mathbf{U}^*), \end{aligned}$$

where τ is a time step; $\mathbf{L}_h(\mathbf{U})$ is the right hand side operator for the ODE (6); \mathbf{U}^n and \mathbf{U}^{n+1} are numerical solutions at the previous and current time steps, respectively.

3.3. Numerical fluxes

Since the numerical solution has discontinuities at the cells boundaries, the boundary fluxes in (6) are evaluated with the so-called numerical fluxes $\tilde{\mathbf{F}}$ and $\tilde{\mathbf{G}}$ instead of original fluxes \mathbf{F} and \mathbf{G} , respectively. The numerical fluxes are usually computed using the approximate solution of Riemann problem for each quadrature point on each cell-to-cell boundary (edge). This approach is usually referenced to as Godunov-type scheme.

In this paper, we imply the idea of coordinate system rotation for each edge in order to use one-dimensional numerical fluxes. In this way, the Local Lax — Friedrichs (LF), HLL and the HLLC approximate Riemann solvers are used. Properties of rotational invariance and hyperbolicity in time for 2D Euler equations (see [14] for details) help to deal with edges that are not aligned with the Cartesian directions. The computation of numerical fluxes through each edge does not depend on the position of the edge in space, hence the source code becomes more simple and flexible. This approach will be significantly more useful in further research for unstructured meshes.

3.4. Limiters

On the one hand, it is clear that high order basis functions in general case should provide a more accurate numerical solution. On the other hand, high order spatial approximation leads to the spurious oscillations in a numerical solution in the neighbourhood of strong discontinuities due to the decrease of scheme viscosity. Non-linear limiters [5, 10] are used to control and suppress such oscillations. For monotonicity purposes we use the MUSCL approach [16] and the Simple WENO (WENO_S) limiter [11].

The simplest way to apply a limitation algorithm is the component-wise operating with the vector of the conservative variables \mathbf{U} . On the other hand, dealing with the so-called local Riemann invariants — alternative variables obtained from \mathbf{U} by using the local characteristic decomposition of the matrices (4) of the quasilinear equation form — allows to improve a numerical solution, however it increases significantly the computational cost of the whole procedure [12]. The computational cost makes characteristic approach useless for the MUSCL which simplicity is one of its benefits. At the same time this approach appears very effective for the WENO-based limiters [8]. The approach procedures can be described as follows:

- (i) get the average values \mathbf{U}_j^0 of the numerical solution at a troubled cell I_{tr} ;
- (ii) for each edge e of a troubled cell with an outward normal $\mathbf{n} = \{\cos \theta, \sin \theta\}$:
 - (a) using the calculated average value compute the eigenvectors matrices $\Omega_R(\theta)$ and $\Omega_L(\theta)$;
 - (b) transform the conservative variables into the local Riemann invariants $\mathbf{W}_k = \Omega_L(\theta)\mathbf{U}_k$, $k \in S$, where S is the set of the cells which belong to the reconstruction stencil;
 - (c) apply a chosen limiter to the vector \mathbf{W}_j in component-wise way;
 - (d) transform the result back into the conservative variables: $\tilde{\mathbf{U}}_j^e = \Omega_R(\theta)\tilde{\mathbf{W}}_j$;
- (iii) construct the final result $\tilde{\mathbf{U}}_j$ with area averaging:

$$\tilde{\mathbf{U}}_j^e = \frac{\sum_e \tilde{\mathbf{U}}_j^e |I_e|}{\sum_e |I_e|},$$

where $|I_e|$ is the area of the neighbour cell joint with I_{tr} through edge e .

Most of the well-known limiters decrease the accuracy being mistakenly applied in subregions with a smooth solution. It nullifies the gist of high order solution approximation. Hence the first step of the limitation procedure should be related to the proper detection of the so-called “troubled cells”, *i.e.* the cells, the solution at which needs to be corrected for monotonicity and stability purposes. In this paper, the KXRCF [17] indicator of the troubled cells is used.

4. Test cases

4.1. Acoustic pulse propagation

The first test case is simulation of acoustic cylindrical wave propagation induced by small initial disturbance of density field ρ' . The initial disturbance is located at the center of rectangular domain $[0, L_x] \times [0, L_y]$ and defined as the Gaussian function [18]:

$$\rho'(x, y)|_{t=0} = \epsilon \exp(-2(x - 0.5L_x)^2 - 2(y - 0.5L_y)^2), \quad \epsilon = 10^{-6}.$$

Note, that such acoustic problem satisfies the system of linearized Euler equations (1), defined for small perturbations ρ' , u' , v' , p' of density, velocity and pressure:

$$\begin{aligned}\mathbf{U} &= [\rho', \rho_0 u', \rho_0 v', \rho_0 w', p']^T, \\ \mathbf{F} &= [\rho' u_0 + \rho_0 u', \rho_0 u_0 u' + p', \rho_0 u_0 v', \rho_0 u_0 w', u_0 p' + \gamma p_0 u']^T, \\ \mathbf{G} &= [\rho' v_0 + \rho_0 v', \rho_0 v_0 u', \rho_0 v_0 v' + p', \rho_0 v_0 w', v_0 p' + \gamma p_0 v']^T,\end{aligned}$$

where ρ_0 , u_0 , v_0 , p_0 are the reference values of density, velocity components and pressure, respectively.

The pressure distribution satisfies the constant speed of sound $c = \sqrt{\gamma p_0 / \rho_0}$. The reference velocity field is assumed to be zero: $\mathbf{v}_0 = [0, 0, 0]^T$; the reference levels of density and pressure are assumed to be $\rho_0 = 1$, $p_0 = 1$. Sizes of the computational domain are $L_x = L_y = 8$. Boundaries are assumed to be open.

The figure 1 represents the results of computations on the 20×20 cells mesh with the Courant number

$$CFL = \sqrt{\frac{p_0}{\rho_0}} \frac{\tau}{h}$$

equals to 0.2. The solution is shown along the center line $y = Ly/2$ of the square domain at the time moment $t = 2$.

High dissipation rate of the LF flux smooths down the solution, obtained with FVM (Fig. 1a). At the same time, piecewise-linear solution representation seems to be enough to have a good agreement with an analytical solution. The HLL flux usage gives nearly the same results. The significantly less dissipative HLLC flux (Fig. 1b) provides the better solution for FVM. On the other hand, the result for piecewise-linear representation of the solution is not affected by the change of a numerical flux.

Series of computations shows the stability of numerical scheme with the Courant numbers up to 0.25.

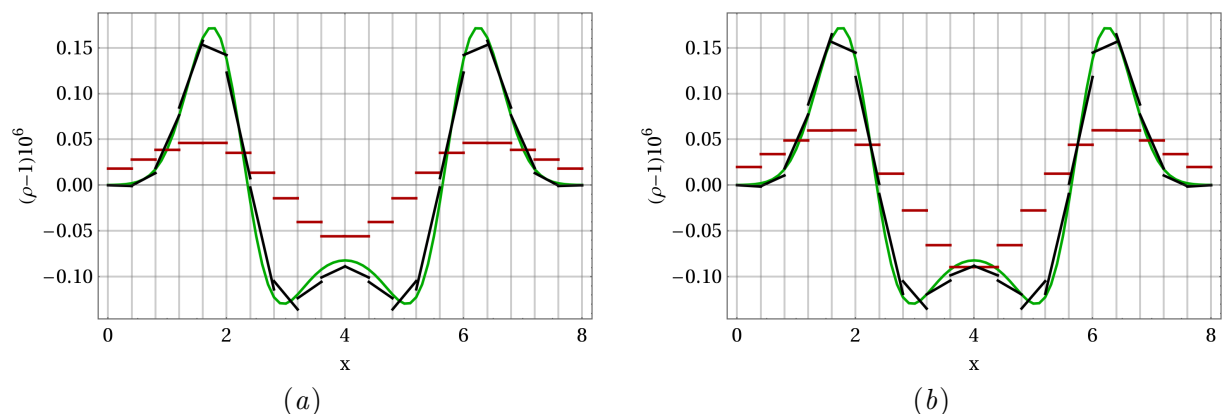


Figure 1. Propagation of acoustic pulse, mesh resolution 20×20 cells, $CFL = 0.2$, density plot along the center line in x -direction, $t = 2.0$: (a) LF numerical flux, (b) HLLC numerical flux. Black line is the piecewise-linear solution (3 basis functions), red line is FVM solution (1 basis function), green line is the analytical solution.

4.2. The Sod problem

Another group of tests is based on modelling of the Sod problem with all three common types of discontinuities: shock wave, rarefaction wave and contact discontinuity. A resolution quality

of these features depends on the sensibility of a troubled cells indicator besides methods of limitation and numerical fluxes, as it will be shown below.

The first test is the simulation in “quasi-one-dimensional” case. The solution is assumed to propagate along the x -axis, the width of a computational domain in y -direction equals one cell only. Initial conditions for this problem are following:

$$(\rho, u, v, w, p) = \begin{cases} (1, 0, 0, 0, 1), & x \leq 0.5, \\ (0.125, 0, 0, 0, 0.1), & x > 0.5. \end{cases}$$

The following results are obtained using the mesh with 100 cells in x -direction and the Courant number equals 0.1, computations are carried out until the time moment $t = 0.2$. This set of parameters is consistent with the one in 1D tests (see [8, 9]).

The first group of results (Fig. 2) demonstrates solutions obtained with the KXRFC indicator of troubled cells and different ways to calculate numerical fluxes and to limit non-physical oscillations. Figure 2a presents the numerical solution of the Sod problem for the MUSCL limiter and the LF numerical flux. These simple tools provide rather monotonous solution with the considerably low resolution of discontinuities: about 6 cells per shock wave and dozen of cells per contact discontinuity. Moreover, there is the lack of accuracy along rarefaction wave and distinctive “hump” in front of it.

The more accurate HLLC flux usage permits to increase the overall quality of the numerical solution (Fig. 2b). This replacement improves rarefaction wave approximation and correspondence between the result and analytical solution in smooth regions despite maintaining numbers of cells per discontinuities.

Replacement of the MUSCL limiter with the WENO_S one leads to more efficient improvement (Fig. 3,4). This limiter provides 2-cell resolution of the shock wave and 5-cell resolution of the contact discontinuity even with dissipative numerical flux like LF, while it maintains the original compactness of the DG scheme: the stencil includes only the neighbouring cells (Fig. 3a). As in the original WENO approach, spurious oscillations may not disappear completely, but their amplitude decreases with the mesh steps decreasing. One can see such oscillations in the smooth solution regions (between the discontinuities). More accurate Riemann solvers like the HLLC improve the quality of numerical solution (Fig. 3b, 4a).

It should be noted, that the solution monotonicity significantly depends on the troubled cells indication method. Figure 4b shows the result of simulation without any indication. Being applied at every cell, WENO_S limiter provides the much better result, overcoming distinctive hump in front of rarefaction wave and some oscillation in smooth regions. Nevertheless, troubled cells indication considerably decrease the computational cost of limitation procedure, and the KXRFC indicator seems to be suitable because of the relative simplicity of its implementation in multidimensional cases.

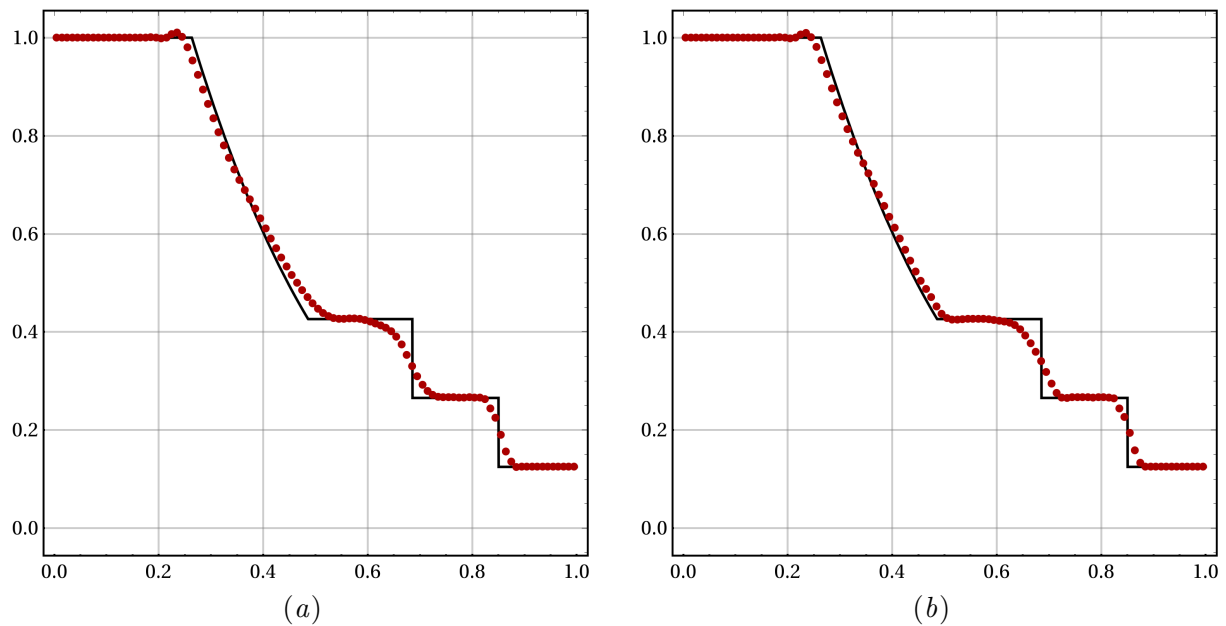


Figure 2. The Sod problem, the density distribution at the final moment of time $t = 0.2$: the analytical solution (black line) and the numerical solution (red dots) obtained with the MUSCL approach, the KXRCF indicator and the numerical fluxes LF (a) and HLLC (b).

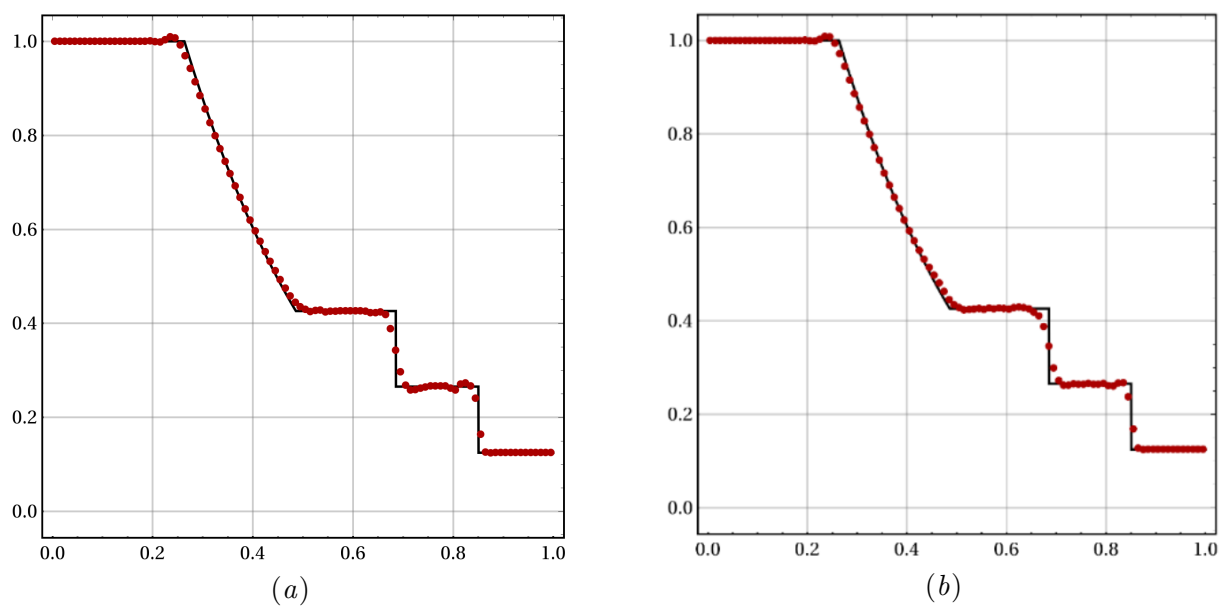


Figure 3. The Sod problem, the density distribution at the final moment of time $t = 0.2$: the analytical solution (black line) and the numerical solution (red dots) obtained with the WENO_S limiter, the KXRCF indicator and the numerical fluxes LF (a) and HLL (b).

The next test is the Sod problem in the unit square where the wavefront is initially placed on the diagonal. Initial conditions for this problem are:

$$(\rho, u, v, w, p) = \begin{cases} (1, 0, 0, 0, 1), & x + y \leq 1, \\ (0.125, 0, 0, 0, 0.1), & x + y > 1. \end{cases}$$

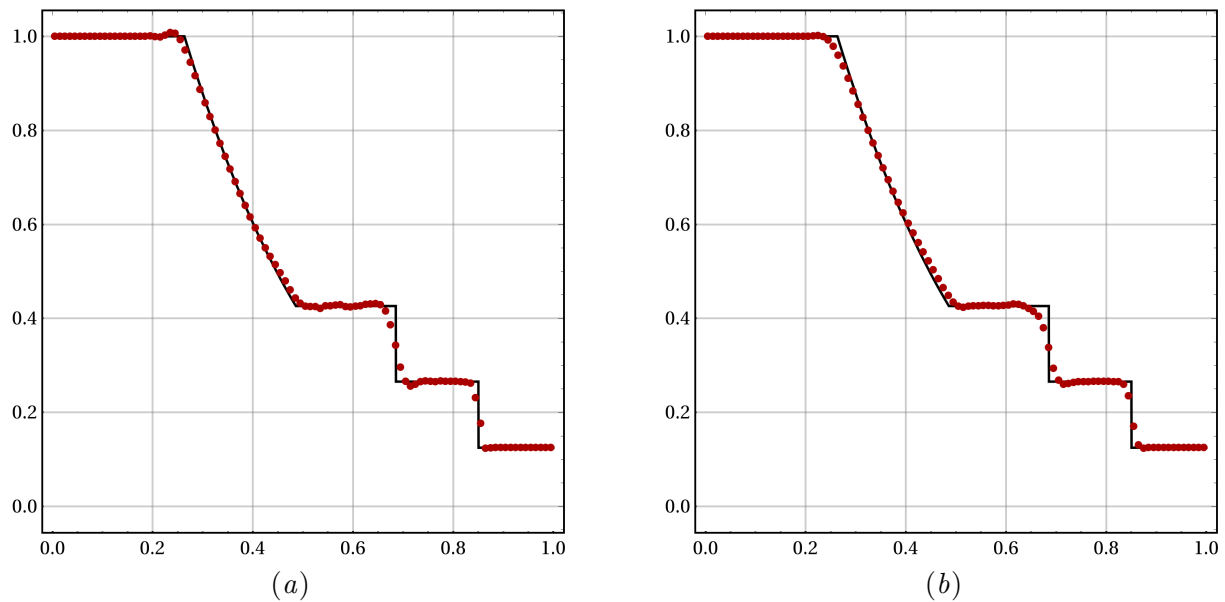


Figure 4. The Sod problem, the density distribution at the final moment of time $t = 0.2$: the analytical solution (black line) and numerical solution (red dots) obtained with the numerical flux HLLC and the WENO_S limiter applied to cells chosen by KXRCF indicator (a) or to all cells (b).

The numerical solution (Fig. 5) is obtained on the 40×40 mesh with the Courant number equals 0.1 until time $t = 0.2$. The HLLC Riemann solver was chosen. Boundaries of the computational domain are supposed to be open, that means zero normal derivatives of the computational variables. This kind of boundary condition leads to the appearance of the spurious secondary waves in subregions near the corners of the square computational domain, caused by the discontinuities at the cells near those corners. Therefore, for efficient comparison between numerical and analytical solutions we consider their sections along the line $x = y$, where the influence of disturbances from corners can be neglected.

The numerical scheme with the MUSCL limiter has high numerical viscosity (Fig. 5a). In opposite, the WENO_S limiter permits to obtain an admissible numerical solution (Fig. 5b). The resolution of discontinuities has the same quality as in “quasi-1D” case.

4.3. Sedov explosion problem

The last test is the Sedov explosion problem involving the propagation of a cylindrical blast wave from a δ -function initial pressure perturbation through the stable medium. This one allows to check the ability of the code to handle strong shocks.

Modelling of this problem is carried out on the unit square domain with the mesh of 200×200 cells and Courant number of 0.2 until $t = 0.1$. Boundaries are assumed to be open. Initial condition for the problem is following:

$$(\rho, u, v, w, p) = \begin{cases} (1, 0, 0, 0, p_{in}(r)), & r \leq \delta r, \\ (1, 0, 0, 0, 10^{-5}), & r > \delta r, \end{cases} \quad p_{in}(r) = \frac{\gamma - 1}{\pi \delta r^2},$$

where $\delta r = 3.5H$ — the radius of the disturbance field, H — the minimal linear cell size.

Figure 6 shows the resulting density distribution computed with HLLC Riemann solver and WENO_S limiter. Handling such a strong discontinuity requires effective limitation technology, because it needs enough numerical dissipation to overcome a spurious oscillations without

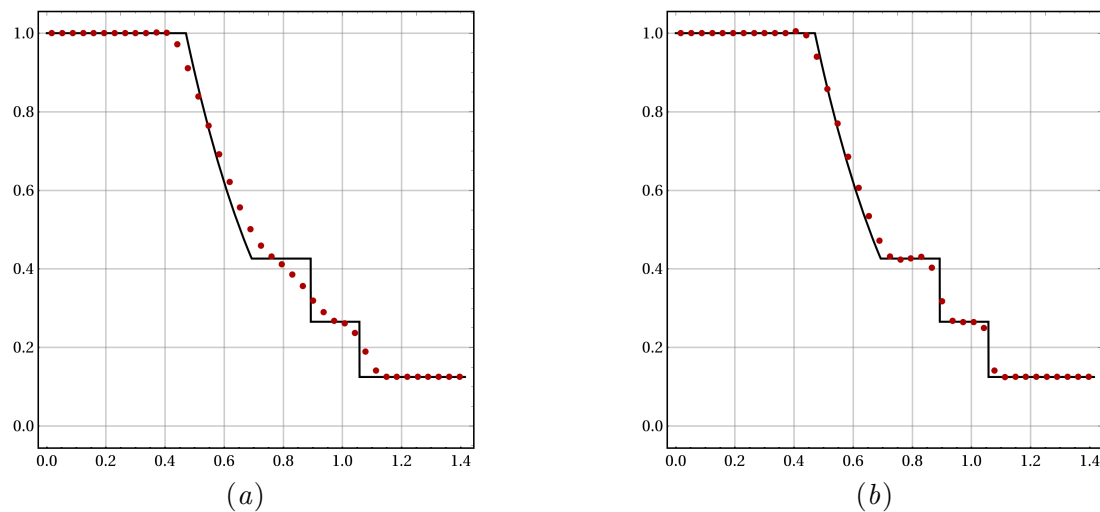


Figure 5. The Sod problem, density distribution along the line $x = y$ in the final moment of time: the analytical solution (black line) and numerical solution (red dots). The calculation with numerical fluxes HLLC and limiters MUSCL (a) and WENO_S (b).

smoothing a shock profile. Current test shows, that WENO_S limiter with the characteristic decomposition provides sufficient monotonicity quality to prevent the blow-up of the code while the limiter itself fails.

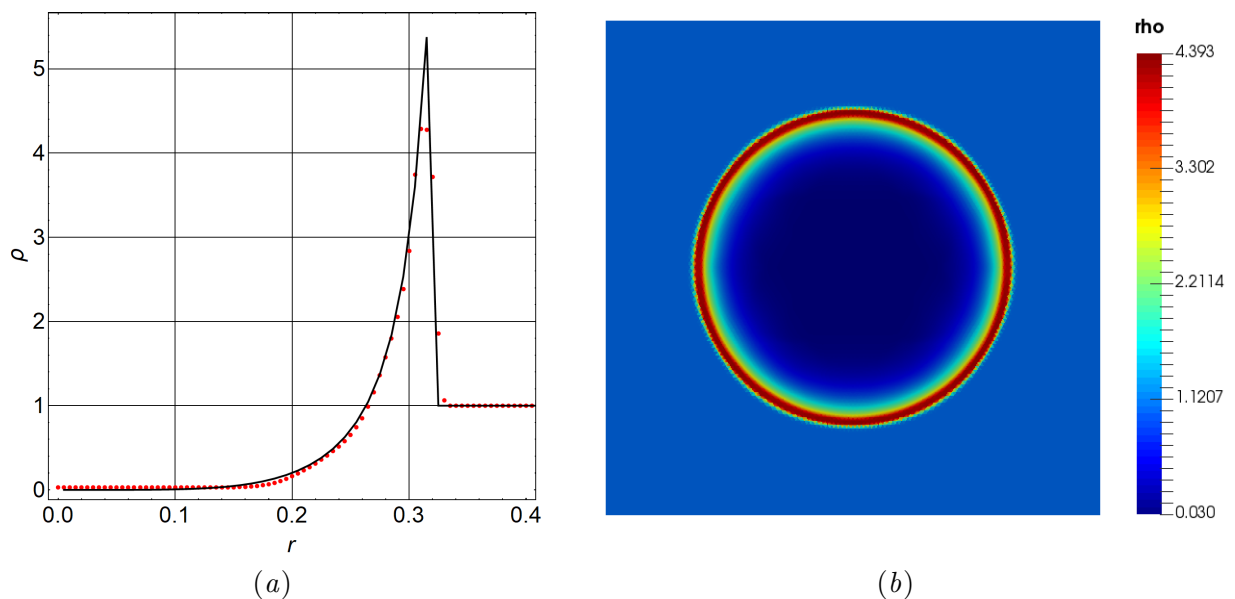


Figure 6. The Sedov explosion problem, density distribution along the radius $y = 0$ (a) and in the whole domain (b) at the time $t = 0.1$; $Co = 0.2$, 200×200 cells mesh in the unit square domain. Black line represents analytical solution, red dots — numerical solution. The calculation with numerical flux HLLC and limiter WENO_S with the characteristic decomposition.

Resulting numerical solution is in good agreement with the analytical solution (fig. 6a). Despite some discrepancy between them on the smooth part, the shock wave takes 3 cells. Figure 6b demonstrates, that the overall distribution of the solution components reflects symmetric nature of the phenomenon.

5. Summary

The RKDG algorithm for 2D gas dynamics problems was implemented in in-house C++ code with the Lax — Friedrichs, HLL, HLLC numerical fluxes, the KXRCF indicator of troubled cells and the WENO_S and MUSCL limiters. Piecewise-linear numerical solution representation in the acoustic pulse propagation problem provides a good agreement with the analytical solution even on rather coarse mesh against the too dissipative FVM results. The efficiency of two implemented limiters has been examined on the Sod problem of discontinuities propagation in the “quasi-1D” case along the x -axis and along the diagonal of a square domain. The numerical scheme with the MUSCL limiter has higher numerical diffusion near discontinuities in comparison with the WENO_S algorithm: 6 vs 3 cells for the shock wave and 12 vs 5 cells for the contact discontinuity representation, respectively. It is shown that the KXRCF algorithm may lead to the non-monotonic solutions: oscillations with small amplitude can arise between the discontinuities. The algorithm can be featured to deal with strong shocks by the limiting of local characteristic variables instead of conservative ones. This modification prevents the numerical blow-up of the Sedov explosion simulation and keeps the high efficiency of the code in terms of the discontinuity resolution quality.

Acknowledgments

The work is partially supported by Russian Foundation for Basic Research (proj. 18-31-20020 and 18-01-00252).

References

- [1] Harris R, Collins E, Sescu A, Luke E, Strutzenberg L and West J 2014 *20th AIAA/CEAS Aeroacoustics Conference* (Atlanta, GA)
- [2] Toulorge T 2012 *Efficient Runge-Kutta Discontinuous Galerkin Methods Applied to Aeroacoustics* Ph.D. thesis Katholieke Universiteit, Leuven
- [3] Bosnyakov I, Lyapunov S, Troshin A, Vlasenko V and Wolkov A 2014 *32nd AIAA Applied Aerodynamics Conference*
- [4] Godunov S 1959 *Math. Sbornik* **47** 271–306
- [5] Cockburn B 1998 *Lecture Notes in Mathematics* **1697** 151–268
- [6] Dimitrienko Y, Koryakov M and Zakharov A 2015 *Mat. Mod. Chisl. Met.* **4** 75–91
- [7] Touze C L, Murrone A and Guillard H 2015 *J. of Comp. Phys.* **84** 389–418
- [8] Galepova V, Lukin V, Marchevsky I and Fufaev I 2017 *Preprints of Keldysh IAP* **131** (Preprint 10.20948/prepr-2017-131)
- [9] Fufaev I N, Lukin V V, Marchevsky I K and Galepova V D 2018 *AIP Conference Proceedings* **2027** 040039
- [10] Qiu J and Shu C W 2006 *SIAM J. Sci. Comput.* **26** 907–929
- [11] Zhong X and Shu C W 2013 *J. Comp. Phys.* **232** 397–415
- [12] Zhu J, Zhong X, Shu C W and Qiu J X 2016 *Communications in Computational Physics* **19** 944–969
- [13] Korchagova V N, Fufaev I N, Lukin V V and Sautkina S M 2018 *AIP Conference Proceedings* **2027** 040049
- [14] Toro E 2009 *Riemann Solvers and Numerical Methods for Fluid Dynamics* (Berlin: Springer)
- [15] Cockburn B and Shu C W 1989 *Math. Comp.* **52** 411–435
- [16] Cockburn B and Shu C W 2001 *J. Sci. Comp.* **3** 173–261
- [17] Krivodonova L, Xin J, Remacle J F, Chevaugeon N and Flaherty J E 2004 *Applied Numerical Mathematics* **48** 323–338
- [18] Tam C and Webb J 1993 *J. of Comp. Phys.* **107** 262–281